Available online at www.CivileJournal.org

Civil Engineering Journal

Vol. 5, No. 5, May, 2019

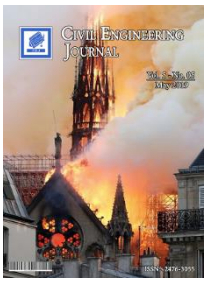

Serviceability Assessment of Continuous Beams Strengthened by SMA Strands under Cyclic Loading

Fatemeh Azadpour [a*], Ali Akbar Maghsoudi [b]

[a] *Ph.D. candidate in Civil Engineering, Shahid Bahonar University of Kerman, Kerman, Iran.*

[b] *Professor, Department of Civil Engineering, Shahid Bahonar University of Kerman, Kerman, Iran.*

Received 19 January 2019; Accepted 23 April 2019

Abstract

Since the wide cracks or large deflections can have a significant effect on the appearance of concrete elements and may cause some uncommon behavior, therefore, serviceability of concrete structures requires investigation. The main objective of this paper is to study experimentally the serviceability of continuous reinforced concrete (RC) beams strengthened by Ni-Ti strands. In addition, some building code provisions were used to calculate crack width and deflection. The current study presents the experimental results to verify the accuracy of building codes' provisions for continuous RC beams strengthened by SMA strands. Although a pattern of smaller width cracks was monitored for strengthened beams, more than 50% of the crack widths were recovered because of super elastic SMA strands. The performance of crack width provisions illustrates an overestimated crack width for SMA RC beams. Moreover, the predicted values for immediate deflections based on building codes provided a good agreement, although the effective reinforcement ratio (steel reinforcement and SMA strands) had a significant effect on immediate deflections of reinforced concrete beams strengthened by SMA strands under service loads.

Keywords: Serviceability; Continuous Beam; Cyclic Loads; Strengthening by Nitinol Strands; Building Codes.

1. Introduction

Nowadays, concrete structures are one of the favorable alternatives in the construction industry and they are considered to satisfy the main criteria of limit states. Well-detailed and properly-erected structures designed by the limit state method will have acceptable probabilities that they will not reach a limit state, will not become unfit for their purpose by collapse and buckling (ultimate limit states), deformation and cracking (serviceability limit states), and therefore, the structure will be durable under environmental conditions over its design life. Some researchers have studied the serviceability requirements, crack width and deflection. Ramos et al. developed and validated a finite element model to study the static and dynamic behavior of a reinforced concrete beam during cracking. A nonlinear behavior was expected at the loading cycle because of cracking. However, upon secondary analysis, when it was loaded again up to the same level, the concrete behaved linearly and so it did not suffer more degradation [1]. Allam et al. investigated building codes formulas and different effective factors for crack width calculations in RC flexural members. Standard codes provisions predicted various values, while Egyptian code underestimated crack width, especially in sections with low reinforcement ratio [2]. Desayi and Ganesan considered a concrete member with a reinforcement bar under tension loading and proposed a new method to calculate crack width. The proposed equation overestimated crack width by 5.1%, while the BS8110 provision underestimated crack width by 18.3% [3]. Rakoczy and Deak theoretically

* Corresponding author: azadpour.f@eng.uk.ac.ir

http://dx.doi.org/10.28991/cej-2019-03091312

investigated the effects of cracked section on deformation of continuous reinforced concrete beams under service limit state. As a result of the proposed method, the plastic redistribution of moments caused a different moment distribution compared to the one assuming constant stiffness [4]. Yasir Alam et al. experimentally tested three different sizes of RC beams to consider crack width and crack spacing under service loads. The results were more or less in agreement with measured values and calculated ones at low strains and small beam size [5]. Araujo presented a nonlinear model as a reference to verify ACI and CEB methods for calculation of immediate and long-term deflections. Both methods showed good results for the uncracked sections and the cracked ones. However, the ACI method is not reliable for deflection calculations related to creep and shrinkage [6]. Shaaban et al. experimentally investigated the crack pattern and deflection of normal strength concrete (NSC) and high strength concrete (HSC) T-beams under service limit state. It was shown that the flange dimensions played an effective role on the beams' behavior. Experimental results demonstrated that the crack initiation was delayed and short-term deflection decreased by increasing the flange dimensions [7].

Although crack width and crack spacing have been widely investigated, plastic deformation of steel reinforcement at unloading can be considered as an important disadvantage of concrete structures, especially when they are subjected to earthquakes. Usage of shape memory alloys, may well solve this problem. Shape memory alloys (SMAs) are innovative materials that have the potential to sustain large deformations and to revert to their undeformed shape upon removing the stress (superelasticity) or by heating (shape memory effect). These unique properties and their particular behavior, especially under cyclic loading, marked them as a desirable material. Shape memory alloys (SMAs) can be formed into different shapes, and therefore, they have the capability of serving various functions: (a) in bridge restrainers for reducing the movement of the deck during an earthquake; (b) Base-isolation systems; (c) in concrete structures for reducing of permanent deformation and also leads to re-centering capacity of the structure after devastation, and (d) in steel structures as a part of the connections or bracing [8].

Saiidi et al. cyclically tested eight simply supported reinforced concrete beams under two-point loading. Half of them were reinforced by Ni-Ti rods. Loading and unloading with half yield load increments were performed until achieving the displacement ductility of two. It was found that the SMA reinforcement had the ability of recovering deformation under cyclic loading [9]. Debbarma and Saha experimentally tested eight simply supported beams, which half of them were reinforced by SMA rods to investigate immediate and long-term deflections. The super elasticity of the SMAs increased loading capacity, resulting in decline of the instantaneous and long-term deflections of SMA RC beams were declined [10]. Choi et al. carried out the bending test on small-scale beams reinforced by four different types of SMA fibers to offer a new method for crack closing. Although all types of SMA fibers increased the flexural strength of reinforced beams, paper-wrapped fibers exhibited higher cracking recovery because of sufficient anchoring action [11]. Khaloo et al. numerically studied the effect of different parameters on cyclic behavior of RC beams reinforced by smart rebars. It was shown that using smart rebars reduced the residual displacement of RC beams under cyclic loading [12]. Shajil et al. carried out three point bending tests on beam specimens in which Ni-Ti fibers were embedded for their self-centering capability. Recoverable deformations were observed under cyclic loading, whereas steel reinforcement rebars could not achieve the small results under similar loading conditions [13]. Nubailah et al. proposed a finite element model to report the behavior of reinforced concrete beams with super elastic shape memory alloys subjected to static loading. SMAs played a positive role on limiting residual displacements and crack propagation. Moreover, SMA RC beams experienced higher yield load and displacement ductility compared to conventional RC beams [14]. Hosseini et al. studied the capability of reinforced concrete structures with shape memory alloys. Copper-based memory alloys and Nickel-based memory alloys were separately used in the stimulated finite element model. It was shown that the rate of general strains and plastic strains in models with Cu-based alloy armatures was higher than those with Ni-based alloy armatures. However, columns with Cu-based alloy armatures experienced less lateral load [15]. Elbahi and Youssef analytically compared the flexural behavior of steel and SMA RC beams during loading and unloading stages, by using a displacement-controlled loading method. The parametric study demonstrated that increasing the SMA bar length reduces the amount of residual displacement and flexural stiffness. Correspondingly, the length of SMA bars played a significant role on the amount of dissipated energy [16].

In spite of various investigations on SMA reinforced concrete sections, their service behavior is currently unknown and needs to be studied. Moreover, since demand of self-compacting concrete (SCC) in the construction industry is growing because of its high workability compared to that of typical vibrated concrete structures, this paper focused particularly on the serviceability of reinforced self-compacting concrete continuous beams strengthened by super elastic SMA strands. As mentioned, previous litarture mainly focused on vibrated concrete and not on SCC.

In this study, four continuous beams were experimentally tested under cyclic loading, which half of them were strengthened by SMA strands in sagging and hogging regions. Based on experimental results, the service response of beams are discussed by the following steps: (i) cyclic loading in increments related to yield deflection, which was measured in a monotonic test [17]; (ii) monitoring the behavior of tensile reinforcements, concrete strains and deflections, and (iii) measuring flexural crack width and deflection under service loads. Likewise, experimental results

are compared with different standards. Figure 1 illustrates the research methodology by a flowchart of the steps used in the current study.

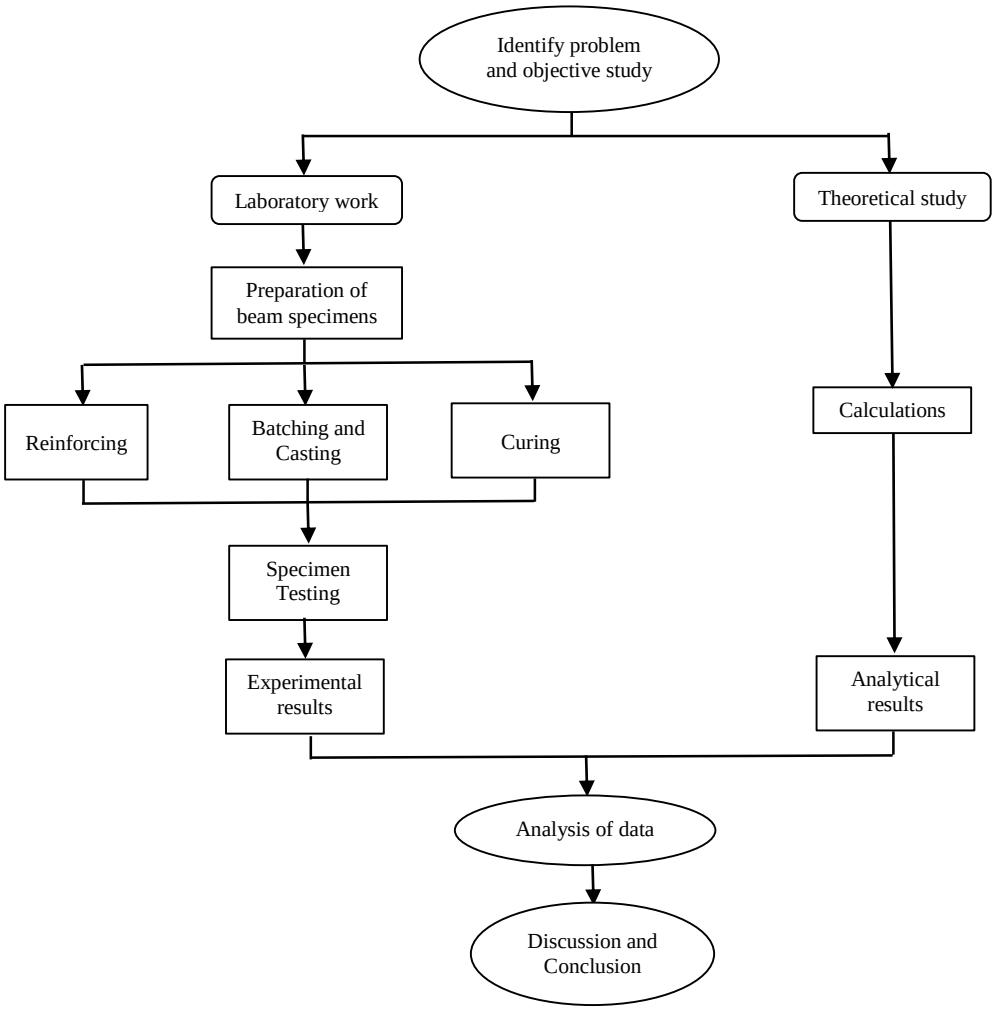

Figure 1. The research methodology

2. Theoretical Serviceability Limit State (SLS) According To Building Codes

2.1. Stress Limitations

Different standards consider service conditions based on the elastic behavior of materials. The limitation of concrete compressive stress is to avoid longitudinal cracks or high level creep where they could result in unacceptable effects on the function of the structure. According to ACI 318M-14 [18], the concrete structures are studied under service loads when the compressive stress in the extreme concrete fiber equals $0.45f_c'$. Considering CSA A23.3 code [19], the limit for the concrete compressive stress in the serviceability limit state is set to $0.4f_c'$. BS8110 [20] explains that in flexural members, the compressive stress should not exceed $0.4f_{cu}$ at the extreme concrete fiber in continuous beams. In EN 1992-2 [21], the compressive stress of concrete is limited to the value $0.6f_{ck}$ under rare load combinations and $0.45f_{ck}$ under quasi-permanent loads. In addition, EN code considered limitations of reinforcement tensile stress to avoid inelastic strain, unacceptable cracking, or deformation. Therefore, the tensile stress of reinforcements is limited to $0.8f_{yk}$ under characteristic load combinations and f_{yk} under an imposed deformation.

2.2. Deflection and Crack Width Considerations

In general, design requirements for the serviceability limit state (SLS) are presented with emphasis on deflection and cracking under service loads. The following deflection and crack width provisions are drawn from different standards.

2.2.1. Crack Width Provisions

i) ACI code

Based on statistical analysis for flexural crack control in beams, Equation 1 predicts the probable maximum crack width [22].

$$W_{max} = (1.08 \times 10^{-5})\beta_h f_s \sqrt[3]{d_c . A} \quad (1)$$

Further researches and experimental works showed that there is no clear relationship between surface crack widths and corrosion. Therefore ACI code proposed a simplified equation based on maximum bar spacing in lieu of earlier crack rules. ACI 318M-14 presented Equation (2) for crack width control [18].

$$s = 380\left(\frac{280}{f_s}\right) - 2.5c_c \quad \leq \quad 300\left(\frac{280}{f_s}\right) \quad (2)$$

ii) Canadian standard

According to CSA A23.3-14 [19], the spacing between the tension bars was considered as the crack width control. Therefore, flexural bars shall be spaced in the tension zone so that the value z in Equation 3 does not exceed 30000N/mm for interior exposure and 25000N/mm for exterior exposure.

$$z = f_s \sqrt[3]{d_c . A} \quad (3)$$

iii) British standard

Based on general provisions of crack width in BS 8110-1997[20], flexural crack width at a particular point on the beam surface depends on a) the concrete cover b) the distance of the neutral axis from the particular point and c) the average surface strain at the considered point. It is declared that the surface crack width, which is calculated from Equation 4 should not exceed 0.3 mm for the visible members (appearance) and the members in aggressive environments (corrosion).

$$W_s = \frac{3a_{cr}\varepsilon_m}{1+2\left(\frac{a_{cr}-c_{min}}{h-x}\right)} \quad (4)$$

It should be noted that the elasticity modulus of concrete in the calculation of strain should be taken as half of the instantaneous value.

iv) Eurocode 2

According to Eurocode2 (EN 1992-1-1) [21], the following Equation 5 is presented for crack width calculations.

$$W_k = S_{r,max}.(\varepsilon_{sm} - \varepsilon_{cm}) \quad (5)$$

$$bar\ spacing \leq 5\left(c + \frac{\phi}{2}\right) \rightarrow S_{r,max} = 3.4c + 0.425K_1K_2\phi/\rho_{p,eff} \quad (6)$$

$$bar\ spacing > 5\left(c + \frac{\phi}{2}\right) \rightarrow S_{r,max} = 1.3(h - x) \quad (7)$$

2.2.2. Deflection Calculations

i) ACI 318M-14 and CSA A23.3-14

Reinforced concrete members subject to flexure shall be designed to have adequate stiffness to limit deflections or any deformations that could adversely affect the strength or serviceability of the structure. When deflections are computed, deflections that occurred immediately upon loading shall be computed by methods or formulas for elastic deflections.

The immediate midspan deflection (Δ_i) of a two-span beam under concentrated loads (Figure 2) can be derived by Equation 8.

$$\Delta_i = \frac{7PL^3}{768E_cI_e} \quad (8)$$

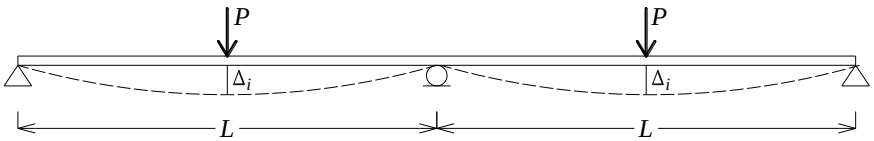

Figure 2. Schematic of a two-span beam under two concentrated loads

For two-span continuous prismatic members, the effective moment of inertia may be taken as the weighted average of the values obtained from Equation 9 for the critical positive and negative moment section. Hence, the average effective moment of inertia can be calculated by Equation 10.

$$I_e = I_{cr} + \left(I_g - I_{cr}\right).\left(\frac{M_{cr}}{M}\right)^3 \leq I_g \quad (9)$$

$$I_{e,ave} = 0.85I_{em} + 0.15I_{eis} \quad (10)$$

The transformed uncracked and cracked section of strengthened beams are shown in Figure 3. Meanwhile, Equations 11-14 were expanded to determine the depth of neutral axis and the moment of inertia for both transformed uncracked and cracked section with SMAs, as follows:

i) Transformed uncracked section

$$\bar{y}_{tr} = (\tfrac{1}{2}B'h + r'd + d')/(1 + B' + r') \quad (11)$$

$$I_{tr} = \left[\frac{1}{12}bh^3 + bh\left(\bar{y}_{tr} - \frac{h}{2}\right)^2\right] + (2n_{st} - 1)A'_{st}.(\bar{y}_{tr} - d')^2 + \\ +[(n_{st} - 1)A_{st} + (n_{SMA} - 1)A_{SMA}].(d - \bar{y}_{tr})^2 \quad (12)$$

ii) Transformed cracked section

$$\bar{y}_{cr} = \left(\sqrt{(1 + r)^2 + 4Bd'(1 + rd/d')} - (1 + r)\right)/2B \quad (13)$$

$$I_{cr} = \frac{1}{3}b\bar{y}_{cr}^3 + (2n_{st} - 1)A'_{st}.(\bar{y}_{cr} - d')^2 + (n_{st}A_{st} + n_{SMA}A_{SMA}).(d - \bar{y}_{cr})^2 \quad (14)$$

Where:

$$B = \frac{b}{2(2n_{st}-1)A'_{st}} \quad ; \quad r = (n_{st}A_{st} + n_{SMA}A_{SMA})/(2n_{st} - 1)A'_{st}$$

$$B' = \frac{bh}{(2n_{st}-1)A'_{st}} \quad ; \quad r' = [(n_{st} - 1)A_{st} + (n_{SMA} - 1)A_{SMA}]/(2n_{st} - 1)A'_{st}$$

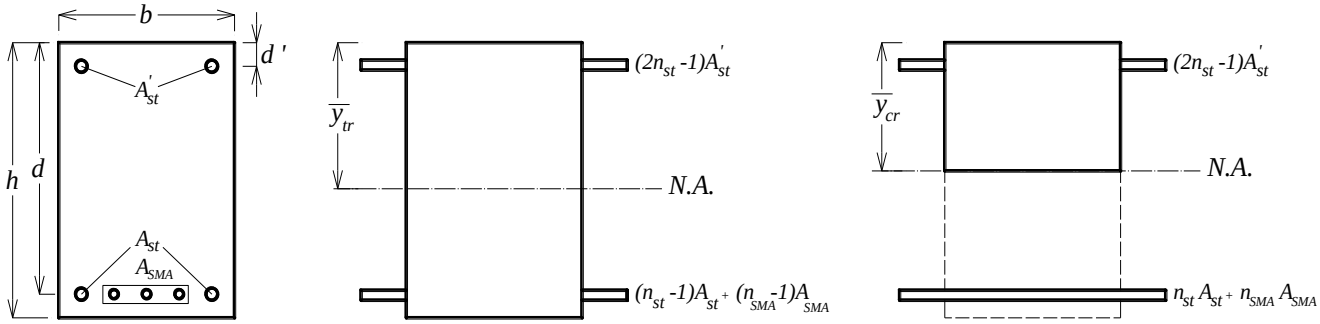

Figure 3. Cross section of strengthened beams: (a) typical section (b) transformed uncracked section (c) transformed cracked section

ii) British standard

According to BS 8110-997 [20], the deflected shape of a member is related to the curvatures, and thus, deflections may be determined by calculating the curvatures at successive sections along the member and using a numerical integration technique. Alternatively, the simplified Equation 15 can be used for calculating deflection based on the curvature.

$$\Delta = KL^2\frac{1}{r} \quad (15)$$

It should be noted that K can be determined by using Equation 16 for the bending moment diagram of continuous beams under concentrated loads (Figure 4).

$$K = 0.083(1 - \frac{M_a + M_b}{4M_c}) \quad (16)$$

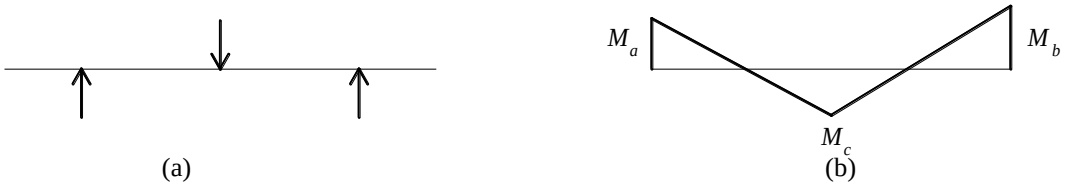

Figure 4. Continuous beam under concentrated loads: (a) loading condition, (b) bending moment diagram

iii) Eurocode 2

In EN 1992-1-1[21], the method of assessing deflections is to compute the curvatures at frequent sections along the member and then calculate the deflection by numerical integration. According to EN, in most cases it will be acceptable to compute the deflection twice, assuming the whole member to be in the uncracked and fully cracked condition in turn, and then interpolate using Equation 17.

$$\alpha = \xi\alpha_{11} + (1-\xi)\alpha_1 \quad (17)$$

$$\xi = 1 - \beta\left(\frac{M_{cr}}{M}\right)^2 \quad (18)$$

3. Experimental Program

3.1. Details of Beam Specimens

Four two-span continuous beams were experimentally tested under cyclic loading up to failure. The beam specimens were designed and casted in two sets of strengthened beams by SMA strands in critical tension regions (BN1-Nm and BN2-Nm) according to the flexural moment diagram and non-strengthened beams (BN1-S and BN2-S), and control beams with just conventional steel reinforcements. The numbers 1 and 2 represent the group of beams according to the percentage of tensile bars. In other words, the beams were entitled BN1 are reinforced by four steel bars of Φ8 at top and bottom, while four steel bars of Φ10 are used at top and bottom of the other two beams were named BN2. Also, one additional tensile bar of Φ8 is added to the beam section at central support. Beam dimensions and reinforcement details are shown in Figure 5 and summarized in Table 1.

Table 1. Beam reinforcement details

Group number	Beam type	Section a-a					Section b-b			
		Steel bar	Additional steel bar	SMA strand	ρ	ρ'	Steel bar	SMA strand	ρ	ρ'
1	BN1-S	$4\Phi_8$	None	None	0.0054	0.0054	$4\Phi_8$	None	0.0054	0.0054
	BN1-Nm	$4\Phi_8$	None	3 $strand_7$ (l=200)	0.0054	0.0054	$4\Phi_8$	3 $strand_7$ (l=250)	0.0054	0.0054
2	BN2-S	$4\Phi_{10}$	$1\Phi_8$ (l=500)	None	0.0112	0.0086	$4\Phi_{10}$	None	0.0086	0.0086
	BN2-Nm	$4\Phi_{10}$	$1\Phi_8$ (l=500)	2 $strand_7$ (l=250)	0.0112	0.0086	$4\Phi_{10}$	2 $strand_7$ (l=320)	0.0086	0.0086

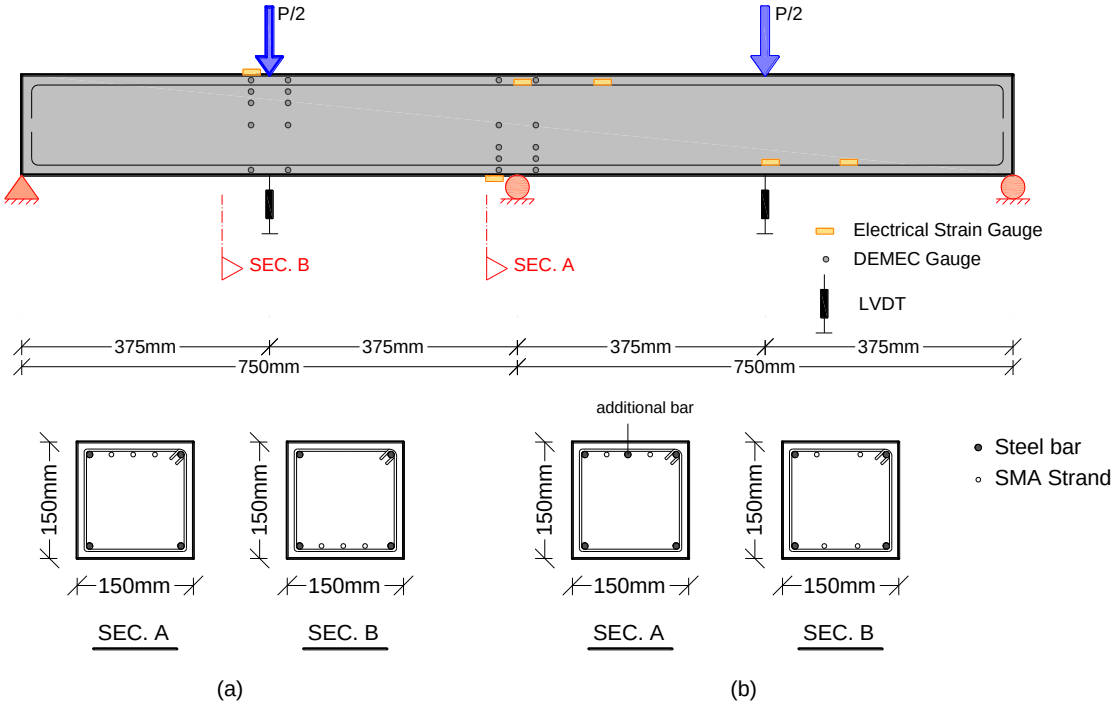

Figure 5. Longitudinal profile and reinforcement details of (a) Group 1; (b) Group 2 (all dimensions in mm)

3.2. Material Properties

The ASTM standard presents some codes considering the required tests for SMA alloys, especially nickel-titanium superelastic materials. The F2004-05 code suggests the differential scanning calorimatory (DSC) method to determine transformation temperatures of superelastic Nitinol materials [23]. The DSC method was implemented and the temperature of phase transformations were measured. According to the DSC diagram given in Figure 6a, the austenite phase will begin at the temperature $A_S = 0℃$ and phase transformation will be completed after obtaining the temperature $A_f = 28℃$ and so the SMA will be completely austenitic. In addition, while it is in a high temperature austenite phase and the material cools down, the austenite to martensite phase transformation will begin at the temperature $M_S = 26℃$ and will become entirely martensitic whenever the temperature reaches $M_f = -7.5℃$. The most reliable method for

stress-strain relationship of Nitinol wires are provided in F2516-07 [24]. Figure 6b shows the derived stress-strain diagram of SMA wires by pulling the sample to 6% strain, unloading to less than 7MPa stress, and then pulling up to failure.

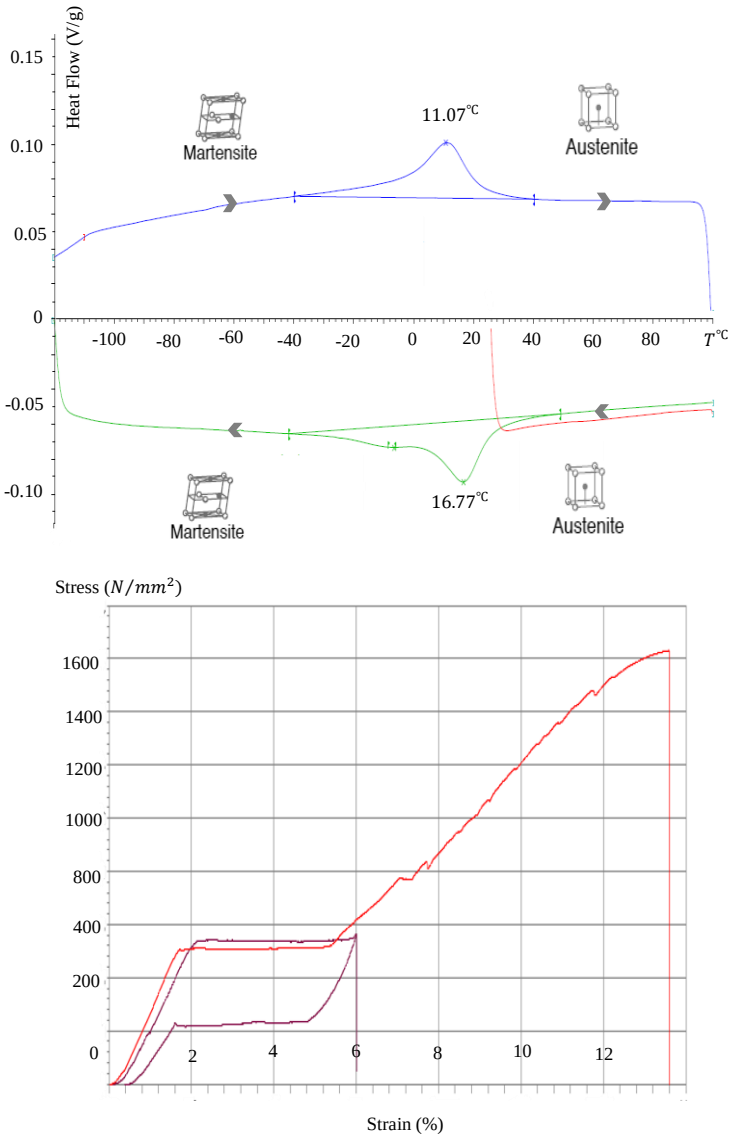

Figure 6. Nitinol wire properties: (a) DSC thermogram; (b) stress-strain diagram

It should be noted that a special machine was used for twisting seven wires to a strand (Figure 7). Likewise, a tension test was carried out on steel reinforcements to determine the required properties. The properties of steel reinforcement and SMA wires such as yield and ultimate strengths and Young's modulus are provided in Table 2. The tested beams were casted with normal strength self-compacting concrete (SCC), while the average of four cylinder compressive strength of concrete at 28 days after casting (f_c') are reported in Table 3.

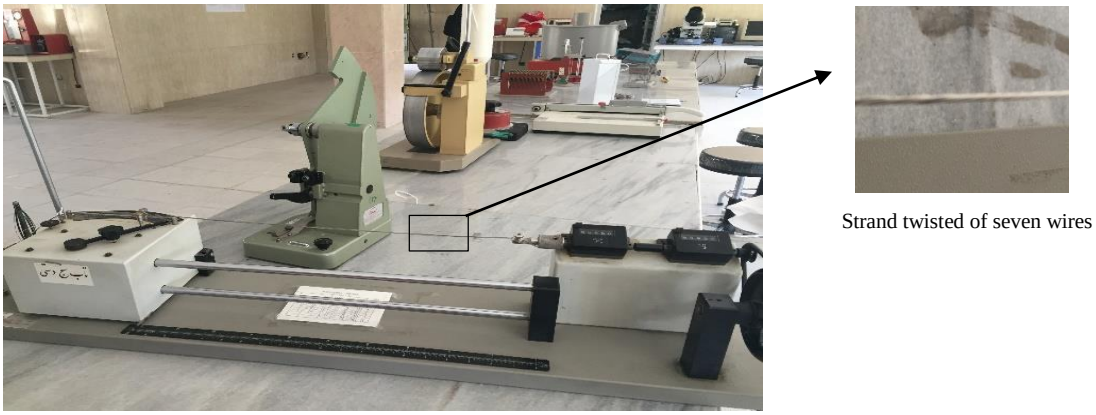

Figure 7. Twisting machine

Table 2. Reinforcement material properties

Type	$f_y(MPa)$	$f_u(MPa)$	$E(GPa)$
Φ_8	371.7	534.0	199
Φ_{10}	323.9	487.7	197
Φ_{12}	324.3	479.4	209
Nitinol wire of 0.46 mm dia.	502.45	1635.56	37.7

Table 3. SCC material properties

Beams specimen	$f'_c\ (MPa)$
BN1-S	43.51
BN1-Nm	36.96
BN2-S	43.56
BN2-Nm	40.65

3.3. Test Setup and Procedure

The test loading procedure of the beams is shown in Figure 8. All specimens were set up as two-span continuous which were loaded by a hydraulic jack. Some electrical strain gauges and DEMEC gauges were attached to different locations of the steel bars and along the height of the beams to monitor the behavior of the specimens during the test (see Figure 5). Meanwhile, vertical deflections of beams at mid-span and central support were recorded by linear variable displacement transducers (LVDTs). A 0.02 mm accurate microscope was implemented to observe the crack widths at every loading and unloading step. The test was conducted cyclically using "displacement control" method. According to ATC-24 [17], the yield values of displacement (Δ_y) were measured from a monotonic loading test. A stepwise displacement cycle is recommended to be applied; which was started as $0.33\Delta_y$ to $1\Delta_y$ in increments of $0.33\Delta_y$ and was continued in increments of $1\Delta_y$ up to the end [17].

Figure 8. Test setup

4. Test Results and Observations

4.1. Cracking Moment

The beams were continuously monitored during the test. While the first visible crack appeared at mid-span, the corresponding force was recorded as the cracking load (P_{cr}) and the experimental cracking moment (M_{exp}) for all tested beams were determined. The cracking moments were also calculated theoretically using Equation 19. It is obvious that the cracking moment of a reinforced concrete member is related to the flexural tensile strength, which is proportional to the compressive strength of concrete. According to Eurocode 2, the flexural tensile strength depends on the mean axial tensile strength (f_{ctm}); in other words, it is a function of the compressive strength.

$$M_{cr} = \frac{f_r . I_{tr}}{y_t} \quad (19)$$

$$f_r = 0.62\sqrt{f'_c} \quad \text{ACI 318M-14 [18]} \quad (19a)$$

$$f_r = 0.3\sqrt{f'_c} \quad \text{CSA A23.3-14 [19]} \quad (19b)$$

$$f_r = max\left(\left(1.6 - \frac{h}{1000}\right) f_{ctm}; f_{ctm}\right) \quad \text{EN 1992-1-1 [21]} \quad (19c)$$

Table 4 provides experimental and theoretical cracking moments for all the tested beams. It is considered that beams strengthened by SMA strands experienced higher cracking moment compared to that of the control beams. In addition, the enhancement ratio of cracking moment (γ) shows an increase of 38% and 15% in cracking moment of strengthened beams, BN1-Nm and BN2-Nm, respectively. Analyzing the ratio of theoretical to experimental cracking moment (M_{cr}/M_{exp}) in Table 4, it is understood that EN 1992-1-1 code had the most conservative prediction of cracking moment with an average theoretical to experimental ratio of 2.77 for the strengthened beams. By contrast, the mean value of theoretical to experimental ratio of cracking moments for beams strengthened by SMA is about 1.056 for CSA, which shows that CSA standard predicts the cracking moment of strengthened beams, unconservatively.

Table 4. Experimental and theoretical cracking moments

Beam	M_{exp} (KN-m)	γ	ACI 318M-14		CSA A23.3-14		EN 1992-1-1	
			M_{cr} (KN-m)	M_{cr}/M_{exp}	M_{cr} (KN-m)	M_{cr}/M_{exp}	M_{cr} (KN-m)	M_{cr}/M_{exp}
BN1-S	0.981	1.00	2.474	2.522	1.201	1.224	3.221	3.615
BN1-Nm	1.138	1.38	2.771	2.435	1.345	1.182	3.650	3.207
BN2-S	1.021	1.00	2.377	2.328	1.157	1.133	2.972	2.911
BN2-Nm	1.178	1.15	2.252	1.912	1.096	0.930	2.748	2.333

4.2. Experimental Stresses under Service States

Standard provisions for allowable stresses (see Section 2.1) were implemented to verify the serviceability state. The permissible strain was calculated according to the elastic behavior of materials under service loads. The material strains were continuously recorded during the test, and therefore, the service load was determined. The results for concrete and steel reinforcement stresses under service loads are summarized in Table 5. It was found that steel stress limitations are critical for the control beam BN1-S, and so, the corresponding loads are measured as the service load in which steel reinforcements obtain their allowable elastic levels. By contrast, the other beams mostly reached their serviceability limit state under concrete stress limitations, and thus, the load was considered as the service load. Meanwhile, all the mentioned codes predict roughly the same service load for the tested beams. In the strengthened beams (BN1-Nm and BN2-Nm), SMA strands were only used in critical tension regions, and therefore, as expected, they had no specific effect on compressive concrete stress. However, the tensile stress in steel reinforcements under service loads declined significantly compared to that of the control beams.

Table 5. Experimental concrete and reinforcement stress under service loads

Beam	Building code	Load (KN)	Loading cycle	$f_s(MPa)$	f_s/f_y	$f_c(MPa)$	f_c/f_c^*
BN1-S	ACI 318M-14	65.13	C3	371.7	1	13.80	0.32
	CSA A23.3-14	65.13	C3	371.7	1	13.21	0.3
	BS 8110	65.13	C3	371.7	1	17.06	0.35
	EN 1992-1-1	62.11	C2	297.35	0.8	10.03	0.23
BN1-Nm	ACI 318M-14	59.68	C4	245.96	0.66	16.63	0.45
	CSA A23.3-14	54.87	C3	257.11	0.69	14.77	0.4
	BS 8110	50.92	C4	201.00	0.54	16.79	0.4
	EN 1992-1-1	57.81	C3	259.30	0.70	16.65	0.45
BN2-S	ACI 318M-14	122.21	C4	302.00	0.93	19.60	0.45
	CSA A23.3-14	115.79	C4	288.81	0.89	17.43	0.4
	BS 8110	103.20	C4	323.90	1	19.13	0.39
	EN 1992-1-1	107.72	C4	259.12	0.8	19.21	0.44
BN2-Nm	ACI 318M-14	83.29	C5	212.17	0.66	18.28	0.45
	CSA A23.3-14	76.45	C5	188.33	0.58	16.27	0.4
	BS 8110	68.60	C4	243.69	0.75	18.32	0.4
	EN 1992-1-1	68.97	C4	259.06	0.8	17.95	0.44

Note: f_c^* is assumed as specified compressive strength of concrete (f_c') in ACI and CSA codes, the cube strength of concrete (f_{cu}) in BS8110 standard and characteristic cylinder strength (f_{ck}) in Eurocode 2.

4.3. Crack Results

4.3.1. Cracking Propagation

Following the guidelines for cyclic testing [17], first, all specimens were loaded up monotonically. The first visible cracks appeared at midspan during the monotonic test. At the end of this step, the cracks were completely recovered in

BN1-Nm and BN2-Nm. By contrast, control beams BN1-S and BN2-S were capable of recovering just 50% of the first crack widths. Loading cyclically, existing midspan cracks became wider and some new ones appeared at both the point load and central support. Figure 9 shows the crack propagations of the tested beams at the service state. As shown in the figure, the number of midspan cracks was more than that of the central support. Whereas SMA RC beams tend to develop cracks of smaller width compared to the control beams.

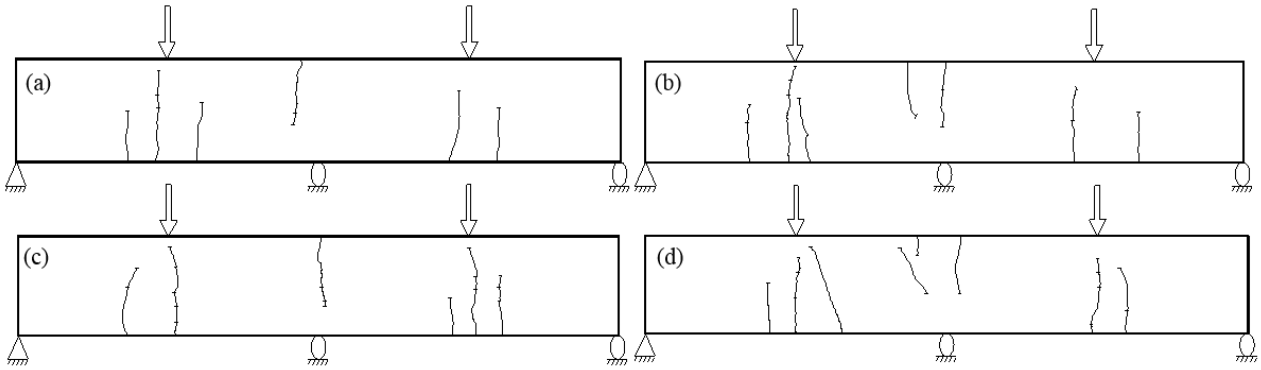

Figure 9. Service crack propagation: (a) BN1-S; (b) BN2-S (c) BN1-Nm (d) BN2-Nm

Table 6 provides the initial and maximum flexural cracking characteristics for the beams tested under cyclic loading. In the conventional RC beams, BN1-S and BN2-S, the first visible flexural crack appeared at approximately 19.43KN and 12.8KN, respectively. At these load levels, both BN1-S and BN2-S had a crack width of about 0.08mm. The superelastic property of SMA strands resulted in smaller width cracks in less cracking load for strengthened beams, BN1-Nm and BN2-Nm. The relative ratio of loads (α) shows a decrease of about 21% and 8% in the cracking load of SMA RC beams, BN1-Nm and BN2-Nm, compared to the corresponding control beams. Considering the reinforcing details of the tested beams, it was found that the increase in reinforcement ratio of SMA RC beams caused less decrease in the amount of cracking load compared to that of conventional RC beams. Moreover, the strengthened beams were found to capable of recovering the initial crack width. At the unloading step, the initial crack in beam BN1-Nm was completely recovered; and the residual crack width in BN2-Nm was negligible (less than 0.01mm). Service crack characteristics such as maximum crack width ($w_{cr,max}$), residual crack width (R_{cr}) and the recovery capacity of crack width are also reported in Table 6. It can be seen that the maximum flexural crack width in the strengthened beams is less than that of nonstrengthened ones. Meanwhile, SMA RC beams recovered approximately 70% and 87% of the crack width under service load. However, less than 50% of crack width were recorded in the control beam.

Table 6. Initial and maximum service crack characteristics

Beam type	Initial flexural crack				Maximum service crack		
	$P_{cr}(KN)$	$W_{i,cr}(mm)$	$R_{i,cr}(mm)$	α	$W_{cr,max}(mm)$	$R_{cr}(mm)$	Recovery capacity
BN1-S	19.43	0.08	0.02	1.00	0.36	0.20	44%
BN1-Nm	15.41	0.04	0	0.79	0.20	0.06	70%
BN2-S	12.8	0.08	0.04	1.00	0.40	0.22	45%
BN2-Nm	11.73	0.04	< 0.01	0.92	0.30	0.04	87%

4.3.2. Assessment of Crack Width Provisions

The crack width provisions of the mentioned standards are applied to the tested specimens and the results are compared with experimental data in Table 7 and Figure 10. Generally, the values of crack widths showed a large scatter among the code equations. As shown, the values predicted by ACI 318M-14 are the highest among those of other codes, although BS 8110 and EN 1992-1-1 mostly predicted similar results for service crack widths. The results obtained from the equations propose an underestimated service crack width for the beam BN2-S, the section reinforced with the ratio of 0.86%. However, ACI 318M-14 was found to provide the best correlation with the experimental service crack width, with the predicted to experimental value of 0.87. In general, ACI 318M-14 predicts more realistic values of service crack width compared to those by other codes.

The values of predicted to experimental ratio are well ranged from -22% to 15% for control beams while those of SMA RC beams indicate that standards provisions overestimated the value of service crack widths for RC beams strengthened by SMA strands. It is a predictable finding because the standards crack width equations were just formulated for conventional reinforced concrete beams. Although a much more logical finding can be achieved by a wide range of experimental data, it is evident that crack width provisions of building codes must be revised for a substantial decline in service crack width of SMA RC beams.

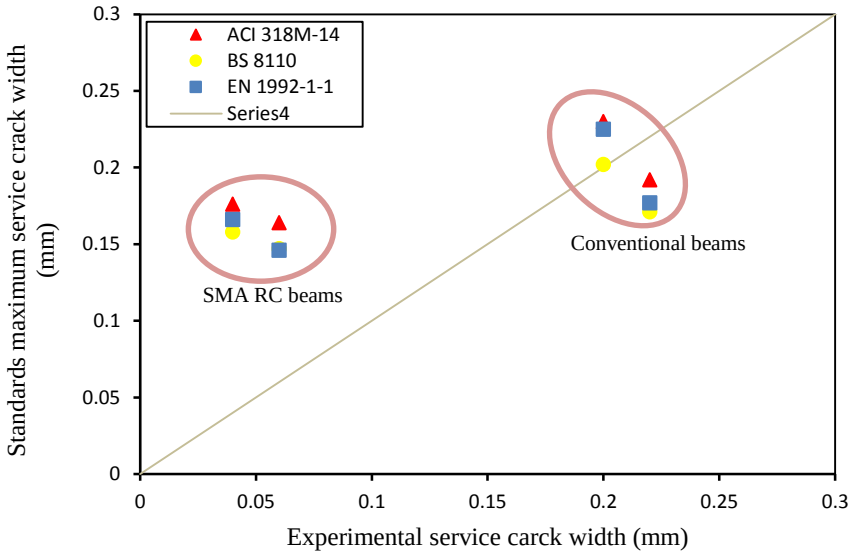

Figure 10. Comparison of maximum crack width based on building codes with experimental maximum crack width under service loads

Table 7. Values of service crack widths based on standards and experimental results

Tested specimen	Maximum crack width (mm)						
	ACI 318M-14		BS 8110		EN 1992-1-1		Experimental
	Eq. (1)	pred./exp.	Eq. (4)	pred./exp.	Eq. (5)	pred./exp.	
BN1-S	0.230	1.15	0.202	1.01	0.225	1.125	0.20
BN1-Nm	0.164	2.73	0.147	2.45	0.146	2.43	0.06
BN2-S	0.192	0.87	0.171	0.78	0.177	0.80	0.22
BN2-Nm	0.176	4.40	0.158	3.95	0.166	4.15	0.04

In SMA RC beams, conventional steel bars and SMA strands were used simultaneously which caused new conditions compared to RC beams with just steel bars. Some particular factors such as steel reinforcement stress and effective reinforcement ratio (conventional steel bars plus SMA strands) affected the crack width in SMA RC beams, which caused narrow cracks to appear. The relationship between experimental service crack width in conventional RC beams and SMA RC beams are shown in Figure 11. The most significant feature of the graph is a dramatic decrease in crack widths under service loads for SMA RC beams. Two groups of beams with the effective reinforcement ratios of 0.56% and 0.88% were experimentally tested. A linear relationship was obtained with the value of service crack width in SMA RC beams and conventional RC beams. The value of service crack width in RC beams strengthened by SMA strands was about 28% and 20% of the corresponding value for RC beams with the effective reinforcement ratio of 0.56% and 0.88%, respectively. On the other hand, the values of the crack widths in SMA RC beams are roughly less than 30% of crack widths in conventional RC beams. Meanwhile, more effective ratio of tension reinforcements caused more narrow cracks in the SMA RC beams.

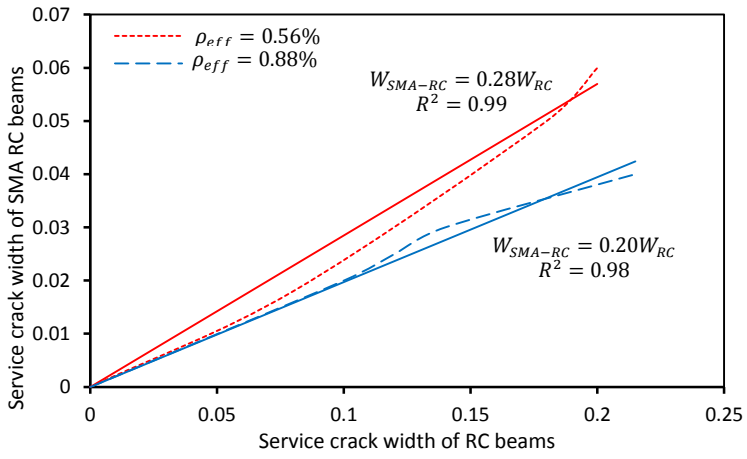

Figure 11. The relationship between observed service crack width in conventional RC beams and SMA RC beams

4.4. Deflection Considerations

4.4.1. Experimental Deflection Behavior

For every loading cycle, the mean value of beam deflection obtained from LVDTs at two midspans are calculated for deflection assessment. The relationship between total applied load and midspan deflection for all tested beams are plotted in Figure 12. Each curve represents the pushover of average midspans' deflection under service loads. It can be seen that maximum service deflection and its residual value for control beams are significantly more than those of the tested beams strengthened by SMA strands. Maximum deflection values of about 1.15 mm and 1.88 mm were recorded for control beams BN1-S and BN2-S corresponding to 83 KN and 130 KN, respectively. Whereas the strengthened beams, BN1-Nm and BN2-Nm, deformed up to approximately 0.62 mm and 1.56 mm corresponding to 58 KN and 100 KN, respectively. While unloading, SMA RC beams BN1-Nm and BN2-Nm were capable of recovering roughly 86% and 69% of maximum service deflection, respectively. However, approximately 58% and 46% of the maximum deflection under service loads recovered in the control beams BN1-S and BN2-S.

As expected, the crack pattern along the beam is different. In turn, the flexural stiffness (EI) has different values based on whether the considered section is cracked or uncracked. The variation of flexural stiffness is directly related to that of the moment of inertia (I); therefore, the ratio of I_e/I_g is used to study the flexural stiffness variation of the tested beams. Figure 13 illustrates the relationship between I_e/I_g and M/M_{cr} at midspan and central support of all the beams. As shown, the I_e/I_g trend of the SMA RC beams is roughly similar to that of the corresponding control beams. However, the strengthened beams experienced lower flexural stiffness for a specific M/M_{cr}. There was a significant decline in the ratio I_e/I_g of cracked specimens until values of M/M_{cr} are less than 2.5 and 1.5 at midspan and central support, respectively. From this point onwards, although the applied moment increased, the ratio I_e/I_g leveled out.

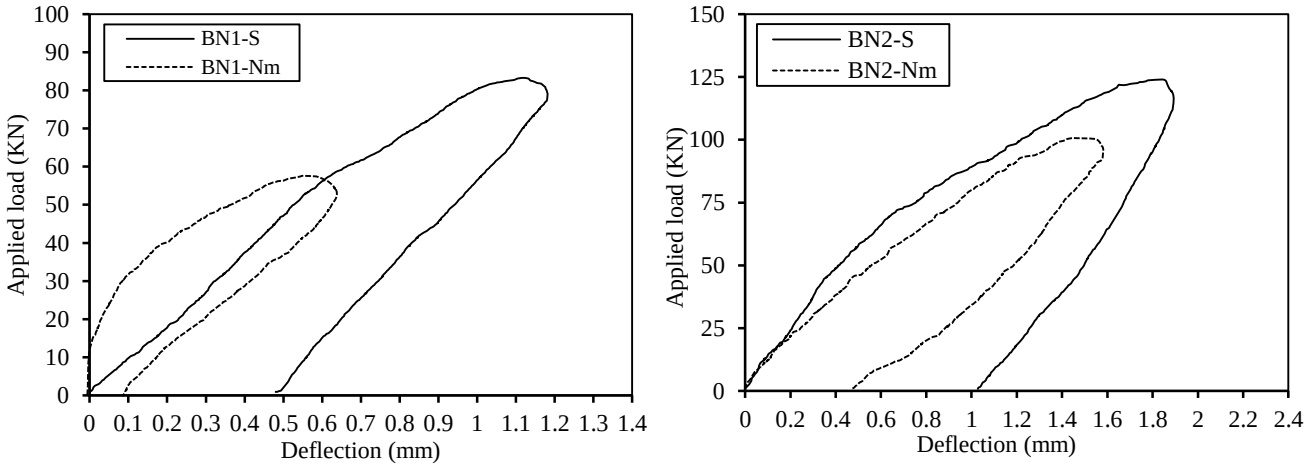

Figure 12. Applied load versus experimental deflection

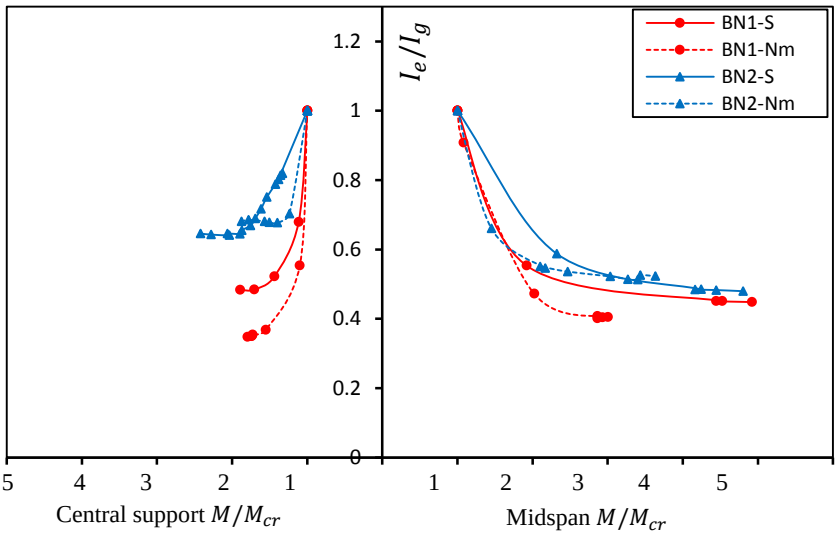

Figure 13. Variation of I_e/I_g versus M/M_{cr} at midspan and central support

4.4.2. Evaluation of Deflection Provisions

According to the mentioned standard provisions (see Section 2.2.2), immediate deflection is calculated at the service limit state. Table 8 provides the predicted deflection (Δ_{pred}), experimental deflection (Δ_{exp}) and the relative ratio of midspan deflection in strengthened beam to that of the corresponding RC beam (γ). Experimental midspan deflections were measured as 0.45mm and 0.97mm in BN1-Nm and BN2-Nm, respectively, and were significantly less than those of the corresponding RC beams. The values of γ demonstrate a decrease of about 50% in midspan deflection of strengthened beams by the SMA strands. In fact, the substantial decline of midspan deflection for SMA RC beams compared with conventional ones are mainly due to their higher displacement ductility, because of their strengthening with superelastic Ni-Ti strands. The values of deflection ratios $\Delta_{pred}/\Delta_{exp}$ (β) are reported in Table 8, and are plotted in Figure 14 for all tested beams in terms of different building codes. As can be seen, the predicted values of ACI 318M-14 and CSA A23.3-14 are approximately the same. Likewise, these two codes predicted the highest instantaneous deflection for beams compared to other building codes. Because of the superelastic property of SMAs, the midspan displacement in SMA RC beams declined compared to that of control beams. Although the decrease of immediate deflection in strengthened beams is clearly obtained from code provisions, the building codes predicted deflection of SMA RC beams, differently. Code provisions conservatively predicted the immediate deflection of beam BN1-Nm ($\rho_{eff} = 0.56\%$) with the value of β ranged between 1.62 and 2.53, whereas the range of β from 0.90 to 1.03 showed an unconservative prediction of instantaneous deflection for beam BN2-Nm ($\rho_{eff} = 0.88\%$). The lower ratio of effective reinforcement demonstrated the more conservative predicted deflection for SMA RC beams. Hence, code provisions for RC beams strengthened by SMAs must be revised with the effective reinforcement ratio in mind. Further tests on this subject are essential.

Table 8. Comparison of measured and predicted immediate deflection

Beam	$\Delta_{exp}(mm)$	γ	ACI 318M-14		CSA A23.3-14		BS 8110		EN 1992-1-1	
			$\Delta_{pred}(mm)$	β	$\Delta_{pred}(mm)$	β	$\Delta_{pred}(mm)$	β	$\Delta_{pred}(mm)$	β
BN1-S	1.09	1.00	1.33	1.22	1.39	1.28	1.10	1.01	1.23	1.13
BN1-Nm	0.45	0.41	1.09	2.42	1.14	2.53	0.92	2.04	0.73	1.62
BN2-S	1.79	1.00	1.95	1.09	2.03	1.13	1.57	0.88	1.39	0.78
BN2-Nm	0.97	0.54	0.96	0.99	1.00	1.03	0.87	0.90	0.89	0.92

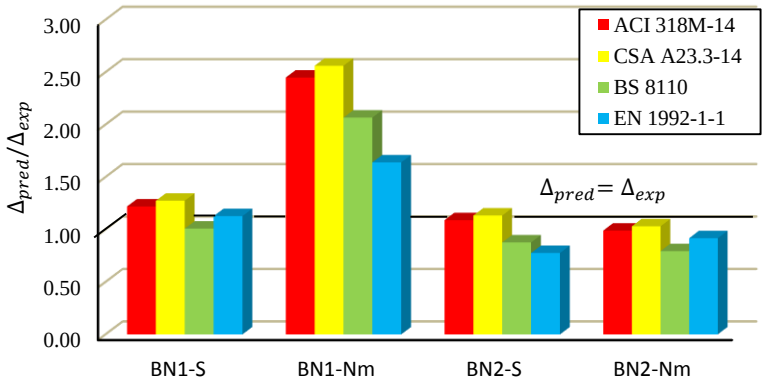

Figure 14. Ratio of predicted to experimental immediate deflection

5. Conclusions

The serviceability of two-span reinforced concrete beams strengthened by SMA strands under cyclic loading was investigated experimentally. Different building codes were also used to assess the service response of strengthened beams such as crack width and deflection. The main results were obtained as follows:

- Unique superelastisity of Ni-Ti strands influenced the concrete pre-cracking stage. Therefore, the cracking moment of RC beams strengthened by SMA strands increased significantly up to 40%. However, theoretical equations predicted higher values of cracking moment compared to experimental data.
- Material strains were monitored continuously during the test to determine service loads. In addition, different building codes were implemented to specify the allowable stress of materials (concrete and steel reinforcement) at service limit state. It was found that RC beams mostly reached to the serviceability limit state under steel reinforcement limitations. By contrast, using SMA strands in strengthened beams caused a substantial decline in steel reinforcement stresses and so concrete stress was highlighted as the service level.

- Considering crack propagations under service loads, smaller width cracks were developed in SMA RC beams compared with control beams. Likewise, SMA RC beams were capable of recovering more than 50% of the service crack widths. On the other hand, theoretical crack widths illustrate that crack width provisions of building codes overestimated the crack widths under service loads for SMA RC beams.
- Experimental deflections of the tested beams showed that the maximum midspan deflection of SMA RC beams was substantially less than that of the control beams. Moreover, RC beams strengthened by SMA strands were able to recover up to 90% of the maximum service deflections.
- Although the I_e/I_g trend of SMA RC beams is roughly similar to that of corresponding control beams, the ratio I_e/I_g of cracked beams decreased substantially for the values M/M_{cr} up to 2.5 and 1.5 at midspan and central support, meaning that the tested beams experienced more cracks. However, for higher values of applied moment, the ratio I_e/I_g remained approximately at the same level.
- Comparison between theoretical deflections based on building codes and experimental data demonstrated a good agreement for the tested beams. However, the effective reinforcement ratio (steel reinforcement and SMA strands) had a significant effect on immediate deflections of reinforced concrete beams strengthened by SMA strands under service loads.

6. Notations

The following symbols are used in this paper:

A	=	Effective tension area of concrete surrounding the flexural tension reinforcement $\left(=\frac{2d_c b}{n}\right)$
A_{st}	=	Area of longitudinal tension reinforcement, mm^2
A'_{st}	=	Area of longitudinal compression reinforcement, mm^2
A_{SMA}	=	Area of longitudinal SMA strands, mm^2
a_{cr}	=	Distance from the particular point to the surface of the nearest longitudinal bar, mm
b	=	Width of beam, mm
C	=	Cover to the longitudinal reinforcement, mm
C_c	=	The least distance from reinforcement surface to the tension concrete face, mm
C_{min}	=	Minimum cover to tension bars, mm
d	=	Effective depth to the centroid of the outer layer of reinforcement, mm
d_c	=	Thickness of cover from the extreme tension fiber to the closest bar, mm
E_c	=	Elasticity modulus of concrete, MPa
E_s	=	Elasticity modulus of steel reinforcement, MPa
E_{SMA}	=	Elasticity modulus of SMA strands, MPa
f_c	=	Design service stress in concrete, MPa
f_{ctm}	=	Mean value of axial tensile strength of concrete, MPa
f_{cu}	=	Characteristic compressive cubic strength of concrete at 28 days, MPa
f_r	=	Modulus of rupture of concrete, MPa
f_s	=	Tensile stress in reinforcement under service loads, MPa
$f_y(f_{yk})$	=	Characteristic yield strength of reinforcement, MPa
f_u	=	Ultimate strength of reinforcement, MPa
$f'_c(f_{ck})$	=	Characteristic compressive cylinder strength of concrete at 28 days, MPa
h	=	Overall depth of the beam, mm
I_{cr}	=	Moment of inertia of cracked section transformed to concrete, mm^4
I_e	=	Effective moment of inertia, mm^4
$I_{e,avg}$	=	Midspan and inner support average moment of inertia, mm^4
I_{eis}	=	Inner support effective moment of inertia, mm^4
I_{em}	=	Midspan effective moment of inertia, mm^4
I_g	=	Moment of inertia of gross concrete section about centroid axis, mm^4
I_{tr}	=	Moment of inertia of uncracked section transformed to concrete, mm^4
K	=	Constant depends on the shape of the bending moment diagram
K_1	=	Coefficient which takes account of the bond properties of the bonded reinforcement
K_2	=	Coefficient which takes account of the distribution of strain

L	=	Span length, mm
M	=	Maximum moment in member due to service loads at stage deflection is calculated, N-mm
M_{cr}	=	Cracking moment, N-mm
n	=	Number of tension reinforcement
n_{SMA}	=	E_{SMA}/E_c
n_{St}	=	E_{St}/E_c
P	=	Applied load, KN
S	=	Center-to-center spacing of longitudinal reinforcement, mm
$S_{r,max}$	=	Maximum crack spacing, mm
$W_{max}(W_s, W_k)$	=	Most probable maximum crack width, mm
x	=	Neutral axis depth, mm
y_t	=	Distance between neutral axis and tension face $(= h - x)$, mm
$\bar{y}_{cr}$	=	Neutral axis depth of uncracked section, mm
$\bar{y}_{tr}$	=	Neutral axis depth of cracked section, mm
z	=	Quantity limiting distribution of flexural reinforcement
$\frac{1}{r}$	=	Curvature at mid-span
α	=	Deformation parameter considered which may be a curvature or a deflection
α_1	=	Value of deformation parameter for uncracked scetion
α_{11}	=	Value of deformation parameter for fully cracked section
β	=	Coefficient which takes account of the influence of the loading duration
β_h	=	Ratio of distance between neutral axis and tension face to distance between neutral axis and centroid of reinforcement $(= (h - x)/(d - x))$
Δ_i	=	Immediate deflection, mm
ε_{cm}	=	Mean strain in the concrete between cracks
ε_{sm}	=	Mean strain in the reinforcement under relevant combination of loads
ε_m	=	Average strain at the level where the cracking is being considered
ξ	=	Distribution coefficient
ρ	=	Tension reinforcement ratio $(= A_{st}/bd)$
ρ'	=	Compression reinforcement ratio $(= A'_{st}/bd)$
ρ_{eff}	=	Combined reinforcement ratio $(= (A_{st} + A_{SMA})/bd)$
ϕ	=	Bar diameter, mm

7. Acknowledgments

The authors acknowledge MIB dental company for providing superelastic Ni-Ti wires, and also express their gratitude to the faculty of Civil Engineering at Shahid Bahonar University of Kerman for providing the laboratory test facilities.

8. Conflict of Interest

The authors declare no conflict of interest.

9. References

[1] Ramos, Ismael Sánchez, Omar Aït-Salem Duque, M'Consuelo Huerta Gómez de Merodio, and Natalia Pozhilova. "Cracking Study of a Reinforced Concrete Beam." Procedia Structural Integrity 1 (2016): 257–264. doi:10.1016/j.prostr.2016.02.035.

[2] Allam S. M., Shoukry M. S., Rashad G. E. and Hassan A. S. "Crack Width Evaluation for Flexural RC Members". Alexandria Engineering Journal, May 2012, 51(3):211-220. doi: 10.2016/j.aej.2012.05.001.

[3] Dessayi P. and Ganesan N. "An Investigation on Spacing of Cracks and Maximum Crack Width in Reinforced Concrete Flexural Members". Journal of Materials and Structures, March 1985, 18(2):123-133. doi: 10.1007/bf02473379.

[4] Rakoczy K. and Deak G. "Analysis of Continuous Reinforced Concrete Beams in Serviceability Limit State". Periodica polytechnic Architecture, 2007, 38(1):11-16. doi: 10.3311/pp.ar.2007.1.02.

[5] Alam S. Y., Lenorman T., Loukili A. and Regoin J. P. (2012). "Measuring Crack Width and Spacing in Reinforced Concrete Members". 7th International conference on Fracture Mechanics of Concrete and Concrete Structures, March 2012: 377-382. HAL Id: hal-00683652.

[6] Araujo J. M. (2005). "Simplified Procedures for Calculation of Instantaneous and Long-Term Deflections of Reinforced Concrete Beams". Revista Engenharia Civil da Universidade do Minho, 2005, 24:57-68.

[7] Shaaban I. G., Saidani M., Nuruddin M. F., Malkawi A. B. and Mustafa T. S. "Serviceability Behavior of Normal and High Strength Reinforced Concrete T-beams". European Journal of materials Science and Engineering, 2017, 2(4):99-110.

[8] Chang W. S. and Araki Y. "Use of Shape Memory Alloys in Construction: a Critical Review". Proceedings of the Institution of Civil Engineers-Civil Engineering, May 2016, 169(2):87-95. doi: 10.1680/jcien.15.00010.

[9] Saiidi M. S., Sadrossadat-Zadeh M., Ayoub C. and Itani A. "Pilot Study of Behavior of Concrete Beams Reinforced with Shape Memory Alloys". Journal of Materials in Civil Engineering, June 2007, 19(6):454-461. doi: 10.1061/(asce)0899-1561.

[10] Debbarma S. R. and Saha S. "Analysis of Instantaneous and Time-Dependent Deflections in Shape Memory Alloy Reinforced Concrete Flexural Members". International Proceedings of Computer Science and Information Technology, 2012, 28:154-160.

[11] Choi E., Kim D. J., Chung Y. S., Kim H. S. and Jung C. U. "Crack-Closing of Cement Mortar Beams Using NiTi Cold-Drawn SMA Short Fibers". Smart materials and Structures Journal, December 2014, 24(1):015018. doi: 10.188/0964-1726/24/1/015018.

[12] Khaloo A. R., Eshghi I. and Aghl P. "Study of Behavior of Reinforced Concrete Beams with Smart Rebars Using Finite Element Modeling". International Journal of Civil Engineering, August 2010, 8(3):221-231.

[13] Shajil N., Srinivasan S. M. and Santhanam M. "Self-Centering of Shape Memory Alloy Fiber Reinforced Cement Mortar Members Subjected to Strong Cyclic Loading". Journal of materials and Structures, August 2012, 46(4):651-661. doi: 10.1617/s11527-012-9923-1.

[14] Nubailah A. H., Muhammad H. I., Azmi I. and Azlan A. "Finite Element Analysis of Smart Reinforced Concrete Beams with Super Elastic Shape Memory Alloy Subjected to Static Loading for Seismic Mitigation". 3rd International Conference on the Science and Engineering of Materials, 2017. doi: 10.1063/1.5034564.

[15] Hosseini M., Beiranvand P., Dehestani A. and Dehestani K. "Shape Memory Alloys and Offering Super-Elastic Property Opportunity in Reinforced Concrete Structures". Archives of Materials Science and Engineering, May 2017, 85(1):5-13. doi: 10.5604/01.3001.0010.1553.

[16] Elbahy Y. I. and Youssef M. A. "Flexural Behavior of Superelastic Shape Memory Alloy Reinforced Concrete Beams During Loading and Unloading Stages". Engineering Structures, February 2019, 181:246-259. doi: 10.1016/j.engstruct.2018.12.001.

[17] ATC, ATC-24. "Guidelines for Cyclic Seismic Testing of Components of Steel Structures". Redwood City, CA: Applied Technology Council: 1992. 57pp.

[18] ACI (American Concrete Institute). "Building Code Requirements for Structural Concrete and Commentary". ACI 318M-14, March 2015, Farmington Hills. MI 48331.

[19] CSA (Canadian Standards Association). "Design of Concrete Structures". CSA A23.3-14, June 2014, Canada.

[20] BSI (British Standard Institution). Structural use of concrete. "Code of Practice for Special Circumstances". BS8110, May 1989: Part2.

[21] Eurocode2 (European Standard). Design of Concrete structures. "General Rules and Rules for Buildings". EN 1992, December 2004: Part1-1, Brussels.

[22] ACI (American Concrete Institute). "Control of Cracking in Concrete Structures". ACI 224R, 2001, Farmington Hills. MI 48331.

[23] ASTM. "Standard Test Method for Transformation Temperature of Nickel-Titanium Alloys by Thermal Analysis". F2004-05, Reapproved 2010, west Conshohocken, United States.

[24] ASTM. "Standard Test Method for Tension Testing of Nickel-Titanium Superelastic Materials". F2516-07, 2007, west Conshohocken, united states.